[Short title + Author Name - P&H title] 17 (2024) 105524

Contents lists available at ScienceDirect

Arabian Journal of Chemistry

journal homepage: www.ksu.edu.sa

Fabrication, bacteriostasis and plant growth properties researches of ultrasmall particle sizes of Ag synergistic with Fe_3O_4/Cu/CuO nanocomposites

Shaobo Guo [a,b], Zhang Dan [a,b], Yanming Qiao [c], Haitao Xu [a], Jiufu Lu [a], Zhifeng Liu [a,b], Juan Shi [a], Xiaohui Ji [a,b,*], Tanlei Zhang [a,*]

[a] Shaanxi Key Laboratory of Catalysis, School of Chemical & Environment Science, Shaanxi University of Technology, Hanzhong, Shaanxi 723000, PR China
[b] State Key Laboratory of Qinba Bio-Resource and Ecological Environment, Shaanxi University of Technology, Hanzhong, Shaanxi 723001, PR China
[c] College of Biological Science and Engineering, Shaanxi University of Technology, Hanzhong, Shaanxi 723000, PR China

ARTICLE INFO

Keywords:
Fe_3O_4/Cu/CuO@Ag
ROS
Bacterial
Antibacterial mechanism
Germination

ABSTRACT

Nano-silver (Ag) with ultra-small particle sizes have strong antibacterial activity because it can pass through the bacterial cell wall and enter the internal environment, causing irreversible damage to bacteria, but the disadvantages such as easy agglomeration and high toxicity alone limit its application. Therefore, In this study, by loading ~ 3 nm ultrasmall particle sizes Ag (QDs) on the Fe_3O_4/Cu/CuO (FC) surface, core–shell type Fe_3O_4/Cu/CuO@Ag nanocomposite (FAN) was created. We used commercially available Bordeaux liquid (BM) as a control and targeted Gram-negative *Escherichia coli* (*E. coli*) and Gram-positive *Staphylococcus aureus* (*S. aureus*) to investigate the antibacterial activity of the material and its antibacterial mechanism. To examine the biocompatibility of materials with human cells and their effect on plant growth, the model plant employs mung bean as its objectives. The results showed that FAN can effectively inhibit *E. coli* and *S. aureus* for up to 99.99 % within 20 min, which is ten times greater than BM. It had a delaying effect on the adaptation period and logarithmic phase of bacterial growth, and could effectively destroy bacterial cell walls and respiratory enzymes. According to biocompatibility studies, FAN has little effect on lactation cells and can promote mung bean germination, root growth, and chlorophyll content with twice the efficiency of BM. This research opens the door to inhibition agents for bacterial control in applications.

1. Introduction

Cu^{2+} and Ag^{+}, the principal components of commercially available inorganic antibacterial treatments such as Bordeaux liquid (BM), copper hydroxide, copper sulfate basic, and Mai shu-bao (Ag ion bacteriostatic agent), are frequently utilized in disease prevention due to their potent bactericidal properties (Yeon et al., 2022; Yu et al., 2022), because if they frequently have minor side effects on the human body, safety, and dependability. A specific concentration of Cu ion as a biological trace element not only promotes the growth of plant roots, stems, leaves, and fruits, but also has a potent inhibitory impact on Gram-positive bacteria, Gram-negative bacteria, fungi, viruses, and so on (Nieto et al., 2022; Nilanjan et al., 2022; Liu et al., 2022). However, the increased usage of Cu-based bacterial inhibitors resulted in substantial negative impacts of bacterial drug resistance, which caused significant losses in agricultural production as a result of the rising need for food resulting from population growth.

Numerous studies (Sen et al., 2022; Cao et al., 2022) described the use of organic bacteriostatic compounds to target the functional proteins or active enzymes of bacteria in order to synergistically boost antibacterial action. However, these chemicals are incapable of causing irreversible harm to bacteria. Importantly, the majority of organic compounds in the environment are difficult to breakdown, making it easier for them to linger in plants and cause environmental and human harm. In agricultural development, there is an urgent need to develop a more effective, non-resistance, and less toxic antibacterial agent.

Compared to use Cu^{2+}, Ag^{+} and organic bacteriostatic compounds, Copper nanoparticles (NC) and nano Ag nanoclusters (NAs) have

Peer review under responsibility of King Saud University.
* Corresponding authors.
E-mail addresses: jixiaohui@snut.edu.cn (X. Ji), tianlei@snut.edu.cn (T. Zhang).

https://doi.org/10.1016/j.arabjc.2023.105524
Received 25 June 2023; Accepted 4 December 2023
Available online 10 December 2023

attracted increasing attention in recent years due to their excellent antibacterial activity and no drug resistance. NC and NAs have abundant surface plasmon, and after absorbing a certain amount of light quantum, the electronic transition creates Cu^{2+}, Ag^{+} and reactive oxygen clusters (ROS) (Li et al., 2022; He et al., 2022; Belmonte et al., 2022; Li et al., 2022). Ultimately, the synergistic action of ROS, Cu^{2+} and Ag^{+} can have remarkable antibacterial activity. Sami et al (Sami et al., 2020). reported that the inhibitory trials of NAs on *E. coli* under diverse settings; under the activation of light, these nanoparticles can cause irreparable damage to *E. coli* and drug-resistant *S. aureus*. As stated previously, their data demonstrated that the inhibitory action of NAs is linked to ROS generation. Jung and colleagues (Jang et al., 2020) used graphene oxide as a carrier and loaded NC and NAs nanoparticles on its surface to study the inhibition of bacteria and biofilms, demonstrating that Graphene oxide@Ag/Cu can produce a strong inhibitory activity against *S. aureus*, *Bacillus subtilis*, *Pseudomonas aeruginosa*, *Salmonella*, and biofilms. the results reveal that the material for the in vitro and in vivo inhibitory mechanism is derived from the correct quantity of ROS generated from NC and the synergistic action of Cu^{2+} and Ag^{+}. Rana and colleagues (Rana et al., 2022) have demonstrated that ROS are hazardous to microorganisms such as bacteria, fungus, mycoplasma, and chlamydia, which, within a particular range, can promote seed germination. The majority of researches have established that both NC and NAs nanoparticles can suppress the growth of bacteria via the formation of ROS. Nanomaterials containing Cu or Ag with higher ROS levels in antibacterial applications and plant growth promotion are still under investigation.

In this work, the redox potential of NAs is greater than that of Fe^{2+} ($E_{(Ag+/Ag)} = 0.80$ V, $E_{(Fe3+/Fe2+)} = 0.77$ V) and the composite with FC can boost the electron migration rate of the material via the Fenton reaction to generate more ROS. Ag QDs were loaded onto the surface of FC to produce the FAN composites, which cannot solve the problem of Ag agglomeration, but have strong antibacterial properties by Fenton reaction. We used commercially available BM as a control and targeted *E. coli* and *S. aureus* to investigate the antibacterial activity of the material and its antibacterial mechanism. To examine the biocompatibility of materials, the model plant employs mung bean as its targets. this FAN multifunctional composite can provide novel ideas for the creation of conventional bacterial inhibitors in agricultural productivity.

2. Materials and methods

2.1. Materials and characterization

Silver nitrate ($AgNO_3$ AR), Iron (III) chloride hexahydrate ($FeCl_3{\cdot}6H_2O$ AR), copper chloride ($CuCl_2$ AR), ethylene glycol (AR), sodium citrate ($C_6H_5Na_3O_7{\cdot}2H_2O$ AR), 3-aminopropyl-trimethylsilane ($C_6H_{17}NSi$ (APTMS) AR), sodium borohydride ($NaBH_4$), sodium chloride (NaCl AR), absolute ethanol (AR), acetonitrile (AR) and isopropanol (AR) were used in this study. Yeast extract powder, tryptone and agar were bought from Beijing Obosing Biotechnology. *E. coli* (NBCC 133264) and *S. aureus* (NBCC 337755) were provided by Shaanxi Institute of Edible Fungi. Water used in all experiments was purified. All chemicals were ACS grade and used as received without further purification.

The morphology and size of the synthesized samples were confirmed using TEM (JEM-2010F, Japan). The XRD analysis of the samples were recorded by X-ray powder diffraction (ADVANCE-D8, Germany), detected in the 2θ range of 20 − 80°. The UV–Visible absorption spectra of the synthesized samples were acquired with a UV–Vis spectrophotometer (UV-6100S, Shanghai) at room temperature. The magnetic measurement data of the as-prepared nanocomposite was investigated using a vibrating sample magnetometer (VSM) (HG-500, America). Using X-ray photoelectron spectroscopy, the elements and valence states present on the surface of the final products were determined. For isothermal microcalorimetry measurements, (Setaram-C80, France) microcalorimeter was utilized. Using an Olympus-IX73 inverted fluorescence microscope (Olympus Corporation), the DNA fluorescent staining of the examined samples was seen.

2.2. Preparation of materials

2.2.1. FC was prepared by hydrothermal method

To form a clear solution, 2.4 mM of $FeCl_3{\cdot}6H_2O$ and 1.2 mM of $CuCl_2$ were added to 20 mL of ethylene glycol, Subsequently, NaAc (1.2 g) and $C_6H_5Na_3O_7{\cdot}2H_2O$ (0.2 g) were added to the previous solution and equally dispersed using ultrasonic vibrations. The mixture was moved to the polytetrafluoroethylene internal bile of a 25 mL stainless steel autoclave, where it underwent a 10 h reaction at 200 °C. It was then cooled to room temperature (Gilroy et al., 2016). The black solid was cleaned multiple times with ultrapure water and ethanol before being dried in a 60 °C vacuum oven for 12 h. Fe_3O_4 preparation of $FeCl_3{\cdot}6H_2O$ is 3.2 M; repeat the preceding procedure without $CuCl_2$.

2.2.2. Preparation of Ag QDs

0.5 mM of $AgNO_3$ and 0.5 mM of $C_6H_5Na_3O_7{\cdot}2H_2O$ were mixed in equal volumes to form a 100 mL solution, After 10 min of stirring, 3 mL of 10 mM $NaBH_4$ was added, and the solution colored brilliant yellow after 30 s.

2.2.3. FC surface modification

50 mg of FC was added to 75 mL of isopropanol and stirred for 20 min, then 0.25 mL of APTMS was added and refluxed for 12 h at 70 °C, After reaching room temperature, the product was washed four times with ultrapure water and stored (Mikel et al., 2022).

2.2.4. Preparation of FAN

The modified FC was added to 20 mL of distilled water, followed by the addition of 20 mL of Ag QDs, After 20 min of ultrasonic treatment, static adsorption for 20 min was repeated. The product was washed multiple times with distilled water and dried at 60 °C for 10 h.

2.2.5. Preparation of NAs

100 mL of diethylene glycol was added to a 250 mL flask and heated at 150 °C for 30 min, Then 1.2 mL of 3 mM NaHS was added and stirred for 10 min, Subsequently, 10 mL of 3 mM HCl and 25 mL of 20 mg/mL PVP (all the above solvents were diethylene glycol) were added and heated to 150 °C for 10 min, Finally, 8 mL of 282 mM CF_3COOAg was added and reacted at 150 °C for 30 min to obtain NAs. The reaction was terminated by cooling in the ice water bath, The NAs was washed three times with acetone at 15,000 r/min, twice with 0.5 % sodium citrate, and dried in a vacuum dryer for further use (Wang et al., 2013).

2.3. Monitoring of ROS production

To monitor ROS generation in nanoparticles, we used ascorbic acid as a monitoring agent (ascorbic acid has a characteristic UV–vis absorption peak at 266 nm and can be oxidized by ROS to non-absorbing deoxyascorbic acid), specifically phosphate buffer (PBS, PH = 7.4) 10 mL was added to nanoparticles and ascorbic acid successively to adjust the final concentration of nanoparticles (16 μg/mL) and ascorbic acid (60 μM). The resulting mixture was incubated at 37 °C for 10 min, remove the nanoparticles by magnetic separation, and ascorbic acid changes were monitored by UV–vis (King et al., 2016; Benarroch and Asally, 2020; Liu et al., 2022).

2.4. Bacteria inhibition experiments (antibacterial activity)

The bacterial inhibitory activity of the materials was monitored with the *E. coli* and *S. aureus*, both of which were grown at 37 °C during their exponential growth phase. The LB medium, ultrapure water, saline, phosphate buffer and other biological materials were sterilized under

autoclave (121 °C, 20 min), and the bacteria were incubated in a biochemical incubator at 37 °C (Deng et al., 2022).

2.4.1. Diffusion experiment of filter paper

The FC, NAs and FAN particles were dispersed in the ultrapure water with sterilization to prepare gradient solutions with concentrations of 50, 100, 200 and 400 μg/mL. The overnight activated bacteria were diluted with sterile saline to 5×10^7 CFU (colony-forming units)/mL, and 500 μL were evenly spread on the sterilized solid LB medium, Then, 8 μL of antibacterial solutions of different materials was added to the LB medium inoculated for 12 h, The observation results of the six groups were done parallel. After obtaining the optimal inhibition concentration, the inhibition activity of the FAN composites was compared with that of a commercially available BM as a reference.

2.4.2. Colony counting experiment

The nanomaterials were added to 5×10^5 CFU/mL bacterial suspension, with a final concentration was 200 μg/mL. The mixture was mixed for 5, 10, 20 and 40 min, respectively, 10 μL of the upper layer liquid was taken and separated using magnetic separation and evenly coated on solid LB medium for 12 h, The results of 6 groups were parallel. The antibacterial efficiency (n) was as follows,

$$\boldsymbol{n} = (\boldsymbol{B_o} - \boldsymbol{B})/\boldsymbol{B_o} \times 100\%$$

where $\boldsymbol{n}$ represents the bacteriostatic efficiency, $\boldsymbol{B_0}$ is the number of colonies in the reference and $\boldsymbol{B}$ is the number of colonies with different materials.

2.5. Bacteria inhibition mechanism experiments

2.5.1. Bacterial growth curve monitoring experiment

In order to detect the specific effects of the materials on the growth stage of the bacteria, microcalorimetric analysis was used to detect changes in the intensity of heat release from bacteria during the acclimation, logarithmic, stabilization and decline periods to analyze the bacterial inhibitory activity of the material, more heat release from bacteria indicates stronger bacterial growth activity. Therefore, the material and the liquid LB medium of the inoculated bacteria were mixed to prepare 5 mL solution. The final bacterial concentration was 5×10^7 CFU/mL, and the material concentration was 200 μg/mL. The growth and heat release intensity of the bacteria were monitored at 37 °C.

2.5.2. Bacterial cell wall potential analysis

In order to further test the extent of bacterial cell wall damage, Zeta potential can be used to measure the change of bacterial cell wall charge to explore the damage of bacterial cell wall. The bacteria was diluted to 7.5×10^7 CFU/mL, more sterile water was added into the material in sequence. The final concentration of material should be 200 μg/mL, Then cultured for 5 and 20 min after separation and removal of the material, were tested bacteria cell wall potential changes.

2.5.3. Bacterial PI staining experiment

To test the integrity of bacterial cell membrane damage, propidium iodide (PI) was used as a DNA-stained dye. 50 μL of PI (50 μg/mL) was added to the above miscible liquids for 15 min in the dark, The mixture was washed three times with phosphate buffer at 13,000 r/min in a centrifuge, and the bacterial damage was observed under a fluorescence inverted microscope.

2.6. In vitro cytotoxicity of the assay

We investigated the biocompatibility of the materials using the standard MTT method, Using PBS as the control, the cell culture medium was HDMEM containing 10 % standard fetal bovine serum, and the medium was changed every day, Cells were cultured at 37 °C with CO_2 concentration of 5 % and humidity of 95 %. The specific experiments were as follows, the cells were added to the 96 - well plate at a concentration of 2000 cells/well and incubated overnight, The medium was removed, and 100 μL of medium containing materials of different concentrations was added. After culturing for 3 days, 25 μL of MTT solution (5 mg/mL in PBS) was added and incubated for for 2 h. The supernatant was removed and 100 μL of DMSO was added to dissolve the Formazan crystals, The medium was sealed and developed overnight. The absorption peak was monitored by a spectrophotometer to evaluate the toxicity $\boldsymbol{W}$ of materials to cells.

The calculation formula is:

$$\boldsymbol{W} = \boldsymbol{OD}(experimentalgroup)/\boldsymbol{OD}(controlgroup) \times 100\%$$

2.7. Growth impact experiments of plants

For seed germination experiments, mung bean seeds were soaked in 10 % (v/v) $NaClO_4$ for 10 min, washed several times with distilled water, and then soaked in distilled water at 4 °C overnight. The soaked seeds were evenly spread in the petri dishes, 20 plants in each petri dish, repeated six times (initial mung bean seeds), and then added into the petri dish with ultrapure water and a mixture of materials with certain concentrations, Germination was observed for 36 h in the greenhouse at 25 °C (Cota et al., 2020; Du et al., 2018).

2.7.1. Tests of root activity and chlorophyll content

The initial mung bean seeds were added to the nutrient solution and cultured at 25 °C until germination, The germinated seedlings were transferred to the nutrient solution, and the materials with a certain concentration gradient were placed in an artificial climate incubator at 25 °C. The humidity was 60—70 %, the illumination time was 16 h/d, and the illumination intensity was 150 μM/s·m^2, After 14 days, the root growth activity and chlorophyll content were tested.

2.7.2. Root activity test

Root growth activity of mung bean sprouts was monitored using the triphenyltetrazolium chloride (TTC) method. 0.5 g of mung bean sprout roots were taken and mixed with 5 mL of TTC solution (4 g/L) and 5 mL of phosphate buffer (0.07 M), in sequence incubated for 2 h at 37 °C in a dark environment, 2 mL of H_2SO_4 (1 M) was added to stop the reaction, and the roots were removed and wiped, The supernatant was further obtained and the amount of tetrazolium reduction was monitored spectrophotometrically.

2.7.3. Chlorophyll content test

0.15 g of the above leaves were ground to powder using liquid nitrogen for 20 min, further immersed in 20 mL of a mixture of acetone and ethanol (v/v = 1:1) for 24 h, The supernatant was taken and the chlorophyll content was measured by spectrophotometer.

3. Results and discussion

3.1. Characterization of materials

Fig. 1a illustrates a schematic of the FAN synthesis process, $CuCl_2$ and $FeCl_3$ were employed as precursors and reduced by ethylene glycol and $C_6H_5Na_3O_7$ at 200 °C to generate Cu^0 and Fe^{2+} composite crystal nucleus in magnetic ferrite, which grew to form spherical clusters. Cu^0 is oxidized to Cu^{2+} in the air, therefore, FN consists of Fe_3O_4, Cu, and CuO. The carrier FN, a metal oxide surface with a large number of hydroxyl groups, may be grafted onto the surface of spherical clusters by APTES dehydration condensation, and FAN was generated by adsorption of ~ 3 nm Ag QDs utilizing the coordination action of the amino group and Ag^0.

TEM was utilized to study the size and shape during the synthesis process. FC (Fig. S1a and d, Supporting Information) is a monodisperse

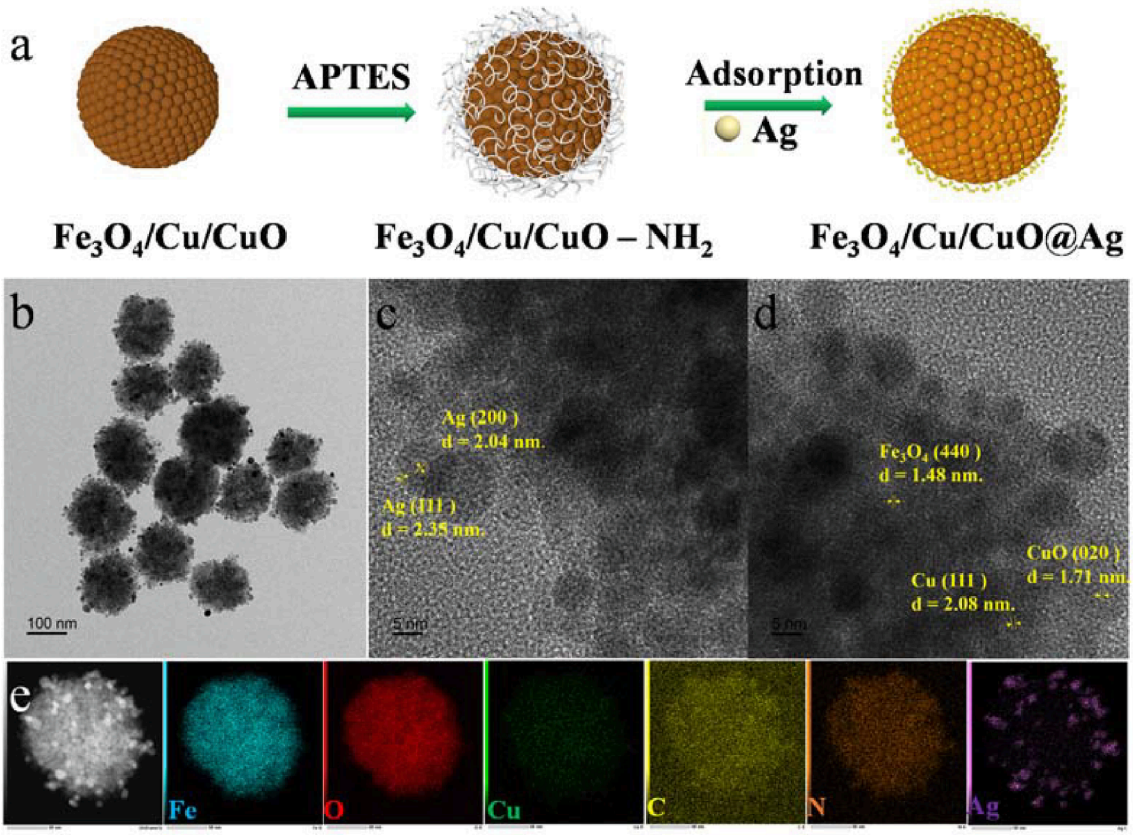

Fig. 1. Schematic illustration of FAN nanocomposite preparation (a). TEM image of FAN (b), Typical HRTEM image of as-synthesized FAN (c, d). Energy dispersive X-ray spectroscopy mapping image of FAN (e).

spherical clusters structure with a particle size of 154.1 ± 18.4 nm, whereas NAs (Fig. S1b, Supporting Information) and Fe_3O_4 (Fig. S1c, Supporting Information) have particle sizes of 8.5 ± 5.2 and 200.8 ± 25.3 nm. FAN (Fig. 1b) composites have a heterostructure with a relatively homogeneous dispersion and a uniform surface loading of 3.0 ± 1.4 nm Ag QDs (Fig. S1e, Supporting Information), respectively, to initially validate the elemental composition of matrix material, Fig. 1c and 1d demonstrates an HR-TEM picture of FAN, the (4 4 0) crystal plane corresponds to the 1.45 nm lattice fringe of Fe_3O_4, whereas the (1 1 1) and (0 2 0) crystal planes correspond to the 2.08 nm and 1.71 nm lattice fringes of Cu and CuO, respectively, the measured lattice fringe distances of Ag are 2.04 nm and 2.35 nm, which correspond to the (2 0 0) and (1 1 1) lattice planes. EDS mapping (Fig. 1e) and spectroscopic plot analysis (Fig. S1f and 1 h, Supporting Information) revealed that FAN contains the elements Fe, O, Cu, N, C and Ag, The results demonstrate that Fe, O, Cu, N, and C are evenly dispersed within the microspheres, while Ag is uniformly placed on their surfaces to produce a heterostructure. The atomic contents of Fe, Cu, Ag, and O are 6.39, 0.65, 0.82, and 22.62 %. The results shown above indicate that Fe_3O_4, Cu, CuO, and Ag are present in FAN, indicating that these three constituents are coupled to form a heterogeneous structure.

X-ray powder diffraction was used to determine the crystal structure of the produced materials, Fig. 2a displays the XRD patterns for NAs, FC, and FAN. The diffraction peaks at approximately 38.9, 44.28, 64.43, and 77.38° correspond to the (1 1 1), (2 0 0), (2 3 0) and (3 3 1) crystal planes of Ag lattice (standard diffraction peak card JCPDS 04–0783). The diffraction peaks at 30.28, 35.85, 57.30 and 62.57°were assigned to the (2 2 0), (3 1 1), (5 1 1) and (4 4 0) crystal planes of spinel type Fe_3O_4 (standard diffraction peak card JCPDS 19–0629). According to JCPDS card numbers 44–0706 (monoclinic phase) and 04–0836 (cubic phase), the most notable diffraction peaks of CuO and Cu, including (0 2 0), (1 1 3) and (1 1 1), (2 0 0), (2 2 0) were at degrees 53.48, 67.9 and 43.30, 50.43, 74.13°, respectively.

Using XPS, the elemental states and surface composition of the FAN (Fig. S2a, Supporting Information) were investigated, and the binding energy spectral peaks of C, N, Ag, Fe, Cu, O and Si are depicted in Fig. S2b-d, (Supporting Information) and Fig. 2b, 2c and 2e. C1s (284.8 eV), N1s (399.2 eV) and Si 2p (101.76 eV) correspond to the elements in APTES, whereas the spectrum peaks at 368.27 and 373.84 eV correspond to the binding energies of Ag 3d5/2 and Ag 3d3/2 of monomeric Ag, respectively. 724.0, 718.6 and 709.9 eV appearing in Fe 2p1/2, Fe 2p2/3 correspond to Fe^{3+} and Fe^{2+} in Fe_3O_4, 933.54 eV in Cu 2p3/2 is attributed to Cu^0, Cu 2p1/2 and 953.7 eV, and the splitting 943.46 and 940.68 eV corresponding to Cu^{2+}, is due to the release of electrons from Cu^0 in the two spectral peaks at 530.8 and 529.5 eV in the O 1 s spectrum correspond to the binding energies of the O^{2-} elements CuO and Fe_3O_4.

Fig. 2f compares the UV–vis absorption spectra of FC, NAs and FAN composites, FC has a broad absorption peak at 600 nm due to the typical absorption peak of Cu, whereas NAs has a peak at 400 nm due to its characteristic absorption peak. As a result of the surface plasmon resonance of Ag and Cu following absorption of visible light, the heterostructure type FAN has a more pronounced absorption peak from 300 nm to the visible light area (Wu et al., 2022), and the change is more pronounced compared to FC and NAs. The magnetic properties of FC and FAN were studied under VSM at room temperature with an external magnetic field ranging from − 10,000 to 10,000 Oe, and their magnetic properties were reflected by the hysteresis lines in Fig. 2g with MS values of 51.56 and 49.65 emu g^{-1} for FC and FAN. Because Ag is not magnetic and its loading on the surface of FC dilutes its magnetic properties, the comparison reveals that the magnetic saturation intensity of FAN is lower, the VSM research demonstrates that FAN possesses powerful magnetic characteristics.

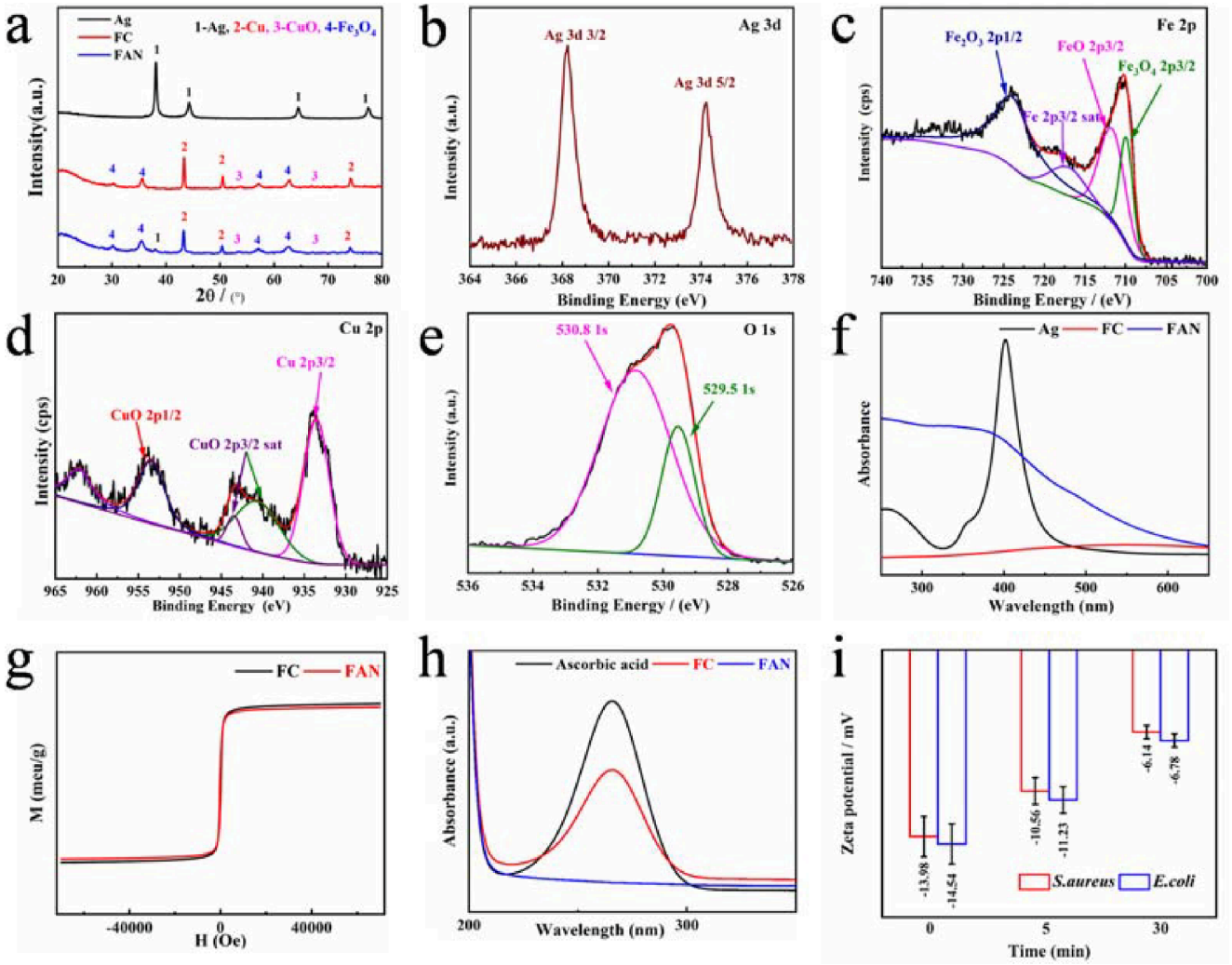

Fig. 2. XRD (a) and XPS spectra of Ag 3d (b), Fe 2p (c), Cu 2p (d), O 1 s (e). UV–vis spectra of FC, NAs and FAN (f). The VSM spectra of Fe_3O_4, FC and FAN (g). UV–Vis diffuse reflectance spectra of FC and FAN samples produces ROS against the degradation peak of ascorbic acid (h). Zeta potential analysis results (i).

Ascorbic acid with a UV–vis distinctive absorption peak was utilized to evaluate the rate of ROS production in order to determine whether FAN produces reactive oxygen species (ROS), The results are depicted in Fig. 2h. After 10 min of incubation, the absorption peak at 266 nm in the reference is the characteristic absorption peak of ascorbic acid, The rate of decomposition was 32.7 % for FC and 99.9 % for FAN. ROS analysis revealed that FAN produced a large amount of ROS in the medium, it was caused by the loading of Ag on the surface of FC, which enhanced the electron migration rate of the nanomaterial.

3.2. Bacteriostatic activity

Bacterial inhibition tests were performed in LB media at 37 °C for 12 h, as shown in Fig. 3a and 3b. The comparison showed no transparent inhibition circle, and Ag NPs had a weak inhibition circle against *E. coli* at 400 μg/mL, but no inhibition activity against *S. aureus*. The inhibitory activity of FC and FAN against microorganisms increased with concentration, the inhibition circle of the two materials against *S. aureus* is greater than that of *E. coli*, indicating that they are more sensitive to *S. aureus*. Furthermore, when two materials of the same strain are compared, FAN has higher inhibitory effect, and the specific diameter ($d \pm 0.1$ cm) of the inhibition circle is displayed in Fig. 3c. When compared to commercially available BM, the best inhibitory concentration was 200 μg/mL, according to data analysis; the findings are displayed in Fig. 4d, 4e and 4f, which shows that at a material concentration of 200 μg/mL, the diameter of the inhibition circle of FAN to *E. coli* is ten times that of BM, whereas that of *S. aureus* is fifteen times that of BM.

The colony counting method was used to evaluate the time inhibition effectiveness and semi-sterilize concentration time (LC_{50}) of the material in order to demonstrate its inhibitory efficiency. As depicted in Fig. 4a and 4d, the bactericidal results of FAN on *E. coli* and *S. aureus* at a concentration of 200 μg/mL at different times revealed that *S. aureus* had almost no colony count in 20 min, indicating that its inhibition rate is 99.99 %, whereas *E. coli*, which contained one colony at the same time, had an inhibition efficiency of greater than 99.98 %. The colony counting method revealed that the inhibition rate against *E. coli* and *S. aureus* reached 99.99 % within 20 min ($LC_{50} = 10$ min) when the concentration was 200 μg/mL.

The findings of the microcalorimetry test for bacterial growth with 200 μg/mL FAN are depicted in Fig. 4g and 4 h. The substance has a delayed effect on the adaptation and logarithmic phase of the bacteria compared to the bacteria in the reference, and the heat flow released is approximately 4 % of that of *S. aureus* in the reference and 13 % of that of *E. coli* in the reference, It has been demonstrated that the substance harmed the respiratory systems of bacteria. Its macroscopic monitoring focuses primarily on heat absorption, which is induced by the combined action of materials and bacteria as bacterial growth metabolism declines. The comparison revealed that the effect of FAN on *S. aureus* was more significant, confirming the preceding findings.

We assessed the change in the potential difference of the bacterial

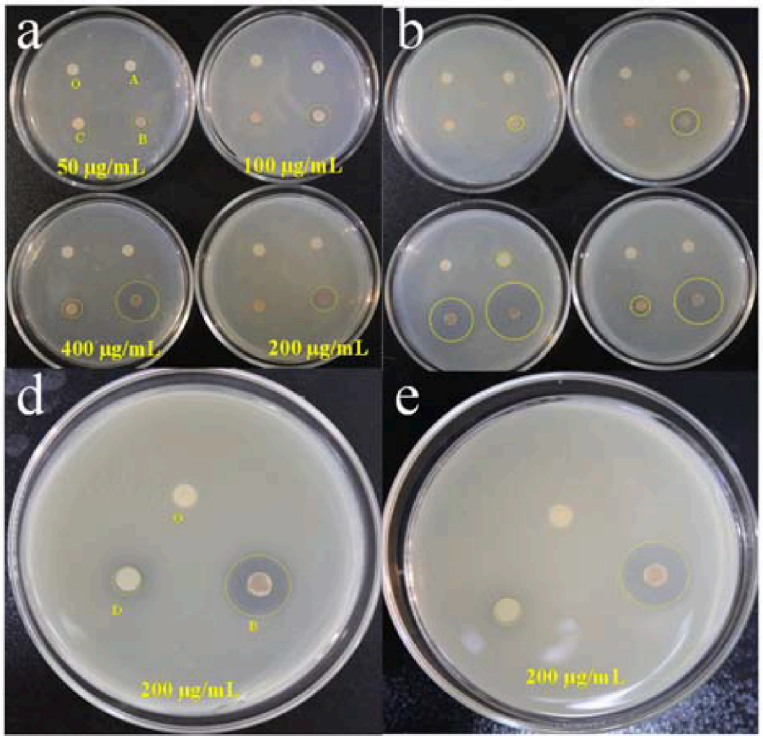

c

C	E.coli (cm)				S.aureus (cm)			
μg/mL	NAs	FC	FAN	BM	NAs	FC	FAN	BM
50	0.00	0.02	0.15	—	0.00	0.05	0.20	—
100	0.00	0.05	0.36	—	0.00	0.12	0.54	—
200	0.00	0.11	0.78	0.07	0.00	0.24	1.16	0.08
400	0.10	0.43	1.02	—	0.08	1.28	1.40	—

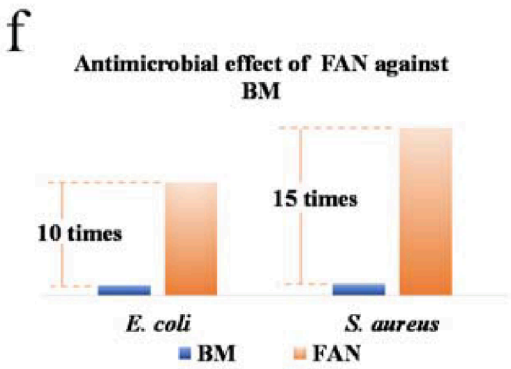

Fig. 3. Photographs of zone of inhibition of *E. coli* (a, b) and *S. aureus* (d, e), O(control), A (NAs), B (FAN), C (FC), D (BM). The detailed zone diameter of the inhibition test results (relative error within 0.03 cm) of composite materials with different concentration and different condition against *E. coli* and *S. aureus* (c). Antimicrobial effect of FAN against BM (f).

cell wall using Zeta potential analysis to determine the cell wall damage caused by the components (Fig. 2i). The experiment revealed that the Zeta potential values of *E. coli* and *S. aureus* at a bacterial concentration of 7.5×10^6 CFU/mL were −14.54 and −13.98 mV, respectively. After mixing with FAN at a concentration of 200 μg/mL for 5 min, the potential values changed to −11.23 and −10.56 mV, and after mixing for 20 min, they decreased to −6 mV. The comparison reveals that the Zeta potential value of the bacteria did not change significantly after 5 min, that may be related to the adsorption of material on the bacteria, which led to the death of a few bacteria. However, the Zeta potential value changed significantly after 20 min, and when combined with microthermal analysis, it can be demonstrated that the FAN material can cause damage to the negative potential difference of the bacterial cell wall, resulting in the destruction of the bacterial cell wall, ultimately, the death of the bacteria.

To further analyze the bactericidal mechanism of the materials against bacteria, the red fluorescent dye (PI) is used to determine the bacterial mortality rate. *E. coli* and *S. aureus* have macroscopic morphologies that are rod-shaped and spherical, respectively. Since PI staining is ineffective on living bacteria, it binds to plasmids or DNA in the nucleic acid of dead bacteria and appears red under a fluorescence microscope. Fig. 4b, 4c, 4e and 4f show an inverted fluorescence microscopy study revealing less red signal in the reference, which were primarily caused by the aging and death of normal bacteria. There are more red spherical spots on *S. aureus* treated with materials than on *E. coli*, indicating that materials can disrupt *S. aureus* cell wall.

As trace elements of plants and animals, copper and iron ions are similarly hazardous in big concentrations. To examine the cytotoxicity of BM and materials, we utilized MCF-7 cells as the target and employed the semi-inhibitory concentration (IC_{50}) of the commercially available anticancer drug Pictilisib (GDC-0941) as a reference. The results (Fig. 4i) revealed that the IC_{50} of GDC-0941 was 308.18 ± 10.00 μg/mL, BM was 19.58 ± 1.00 μg/mL, and FAN was 209.97 ± 8.00 μg/mL. BM and FAN are approximately two-thirds as hazardous to MCF-7 cells as the commercially available GDC-0941, but the safe concentration is ten times higher than that of BM.

3.3. Analysis of antibacterial mechanism

The Ag QDs included in FAN has an abundant surface plasma, and following absorption of visible light, the electron resonance on the local surface causes the transition of d-orbit electrons into holes and free electrons. The conjunction of holes and oxygen in the medium can form reactive oxygen species (ROS), and electron participation in the cycles of Cu^0, Cu^{2+}, Fe^{2+}, and Fe^{3+} increases the electron migration rate, ROS and trace amounts of Fe and Cu ions may also be released during this electron migration process. The primary distinction between Gram-negative *E. coli* and Gram-positive *S. aureus* utilized as model bacteria is the structure of the cell wall, *S. aureus* cell walls have 40——60 layers of stable phospholipid bilayer structure and a minor quantity of phospholipid acid, whereas *E. coli* cell walls contain a substantial amount of lipopolysaccharide and a tiny amount of phospholipid bilayer (An et al., 2021; Ding et al., 2021). Different levels of PO_4^-, –OH, and COO^- in phospholipid bilayers, phosphopeptides, and lipopolysaccharides create a negative potential difference on the bacterial surface, the ions generated by the nano - Cu and Ag of FAN can be adsorbed on the surface of bacteria via electrostatic action, resulting in changes in the potential difference of the cell wall and bacterial death. ROS possesses powerful oxidative characteristics and can damage bacterial organelles. The cell wall of *E. coli* contains a greater quantity of lipopolysaccharide than phospholipid bilayer, and protein is more sensitive to reactive oxygen species (ROS), therefore FAN destroys the cell wall of *E. coli* more severely, which is compatible with the results of PI staining and zeta potential analyses. $Cu(OH)_2$ is the active component of BM, which is utilized as a bacterial inhibitor. Although the released Cu^{2+} is toxic to bacteria, the plasmid in the cytoplasm of *E. coli* contains sensitive RNA that can produce an extracellular efflux pump system through its own regulation. Intracellular metallothionein, metal chelators, and other

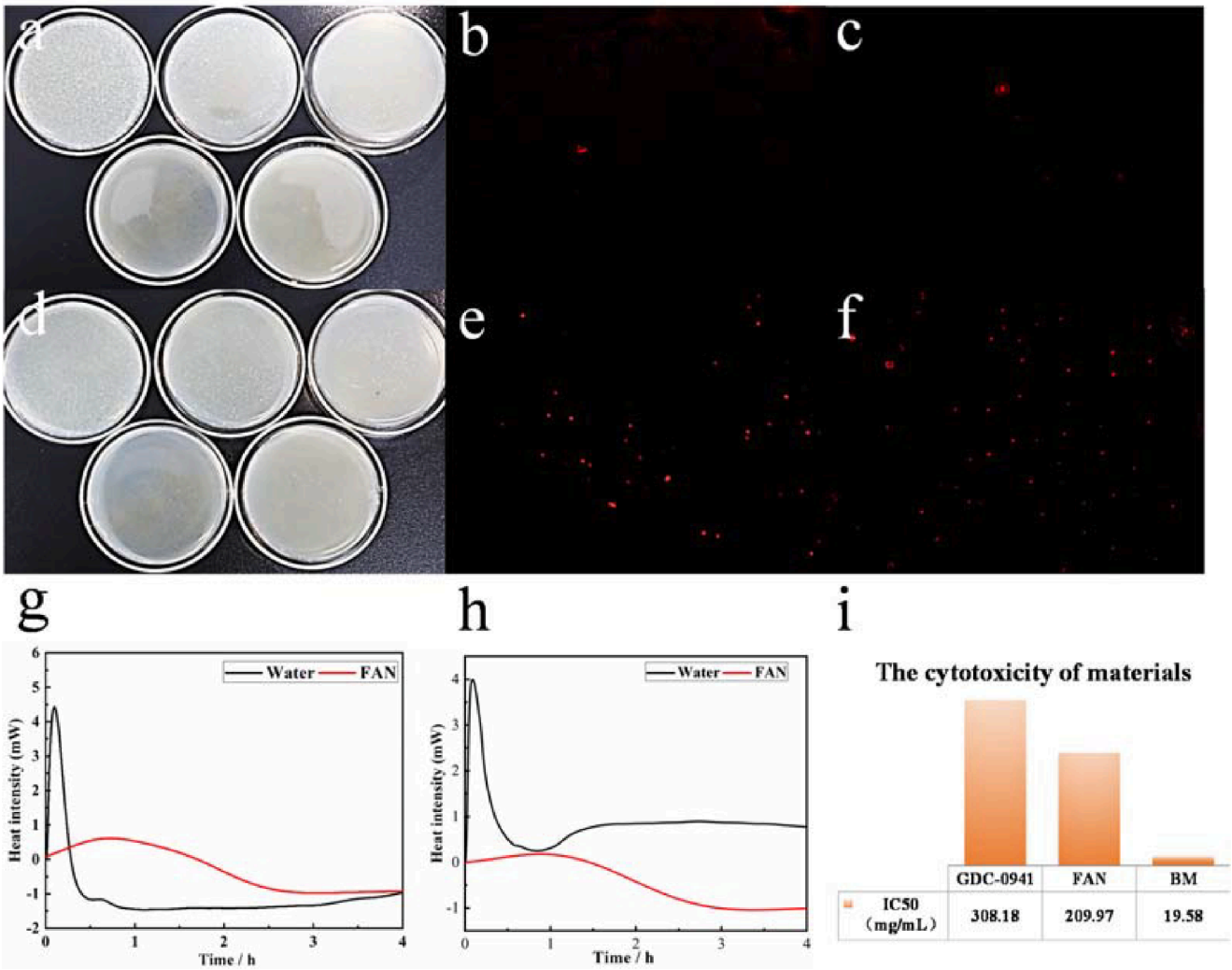

Fig. 4. Images of LB agar culture plate inoculated with *E. coli* (a) and *S. aureus* (d) treated for a short time while inoculated with FAN (200 μg/mL) for 24 h culture. PI staining analysis of FAN on *E. coli* (b, e) and *S. aureus* (c, f). Microcaloric analysis of FAN on *E.coli* (g) and *S.aureus* (h).Viability of MCF-7 cells exposed to GDC-0941, BM and FAN nanoparticles (i).

resistance mechanisms reduce the bacterial inhibitory activity of BM, and additional ROS in FAN can disrupt the efflux pump system in the absence of bacterial resistance (Wang et al., 2022; Imani et al., 2020). Secondly, nano - Ag can enter the bacterial interior through the Cu ion channels (the d orbit of Ag ions is similar to that of Cu ions, and ion channel proteins permit the passage of particle sizes 3 nm free in the cytoplasm (Yu et al., 2020), irreversibly binding Fe-S clusters of metabolic systems in the cytoplasm and releasing Fe^{2+}, which undergoes Fenton reaction in the cytoplasm, and its products can disrupt the normal metabolism of bacteria.(Fig. 5) Despite the fact that the bacteriostatic performance of FAN is superior to that of the BM bacteriostatic mechanism, its mode of action requires additional investigation.

3.4. Effect on mung bean germination

As shown in Fig. 6a, we studied the effect of FAN on the germination structure of mung bean using water as a control and commercially available BM as a comparison. After 36 h of incubation, the root elongation and robustness of seeds in BM at doses of 10, 50, 100, and 200 μg/mL were greater than the control, however root germination was considerably hindered at 400 μg/mL. When the concentration of FAN is between 10 and 200 μg/mL, it clearly promotes the elongation and expansion of the mung bean root system, however above 400 μg/mL, it inhibits litter formation, The inhibitory impact is hence BM > FAN. Under identical FAN and BM concentrations, FAN promoted seed germination with a higher germination rate and a more robust root system than BM.

In this work, mung bean seedlings were used as a model to examine the impacts of materials on root activity and chlorophyll content to better investigate the effects of materials on the physiological indicators of plant seedlings, The growth outcomes are depicted in Fig. 6b and 6c. With reference to the aim, it can be noted that as BM concentration increases, the number of seedling capillary roots increases and the leaves of the plants become more luxuriant, however root activity and leaf growth of bean sprouts are considerably suppressed over 100 μg/mL. At 100 μg/mL, the root activity in FAN did not alter considerably, although the plant chlorophyll content was remained elevated at 200 μg/mL, The root activity and chlorophyll content test results revealed that compared to BM, FAN significantly increased the root activity of mung bean seedlings when the concentration was less than 200 μg/mL, and had a higher chlorophyll content and higher root activity at this concentration, so its application value is double that of BM. Fig. 6d, 6e and 6f depicts the specific growth data analysis results, which are generally compatible with the aforementioned growth outcomes.

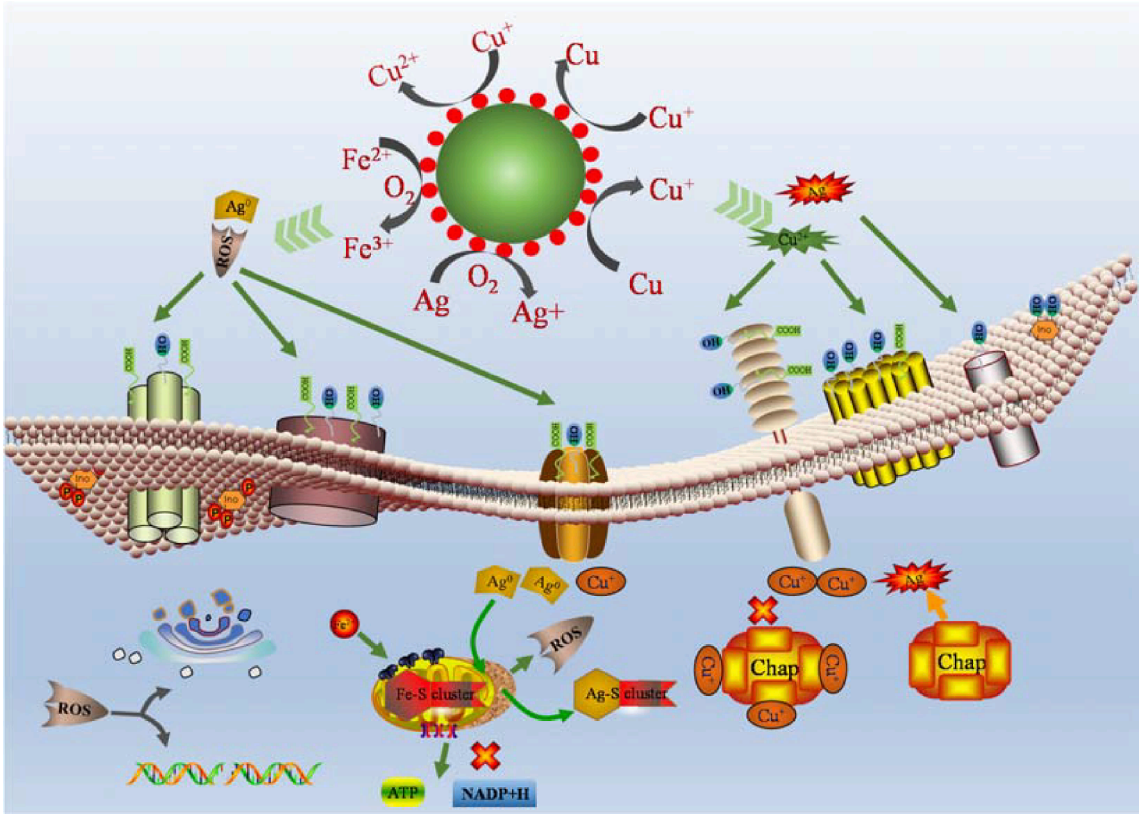

Fig. 5. Antibacterial mechanism diagram.

3.5. Analysis of effects on plant growth

Cu and Fe, which are critical trace elements for plants, are present in the material. In the early stages of seed germination, the seeds undergo anaerobic respiration, and the ROS created by FAN in the medium might oxidize the seed testa, triggering the production of reduced glutathione, this promotes seed germination by boosting the activity of amylase and protease. In addition, during aerobic respiration, the metabolic rate in the root system of mung bean seeds after germination accelerates, the demand for Fe and Cu ions increases, and excess Cu and Fe elements are stored in the cell wall of the roots for the subsequent growth of stems and leaves, allowing the germination process to tolerate higher concentrations of FAN. Although a tiny amount of BM can enhance root growth, the same concentration of Fe and ROS in FAN has a greater effect on stimulating seed germination and growth, therefore, it is evident that FAN has a stronger effect on mung bean. During the growth phase, metal ions are adsorbed on the plant cell wall via electrostatic interaction, after diffusing through the cell wall, they are reduced to effective ions by reductive oxidases, enter the cell interior, and are transported to chloroplasts, mitochondria, vesicles and other organelles by transpiration to participate in plant metabolism. Numerous catalytic enzymes are required to participate in this reaction, because Fe and Cu can participate in photosynthetic catalase, metabolic enzymes, and respiratory enzymes, among other things (Banakar et al., 2017); FAN can enhance plant growth. When Cu ions are used alone, DNA preferentially expresses enzymes involved in photosynthesis related to Cu ions and coerces the activity of acid ester reductase in chlorophyll, which affects the uptake of Fe by plants as a cofactor material for chlorophyll synthesis, whereas Fe deficiency leads to a decrease in photosynthetic capacity, thus reducing chlorophyll synthesis (Fig. 7). More research is needed to understand the specific mechanism impacting chlorophyll metabolism. Simultaneously, excessive Cu causes a large number of ROS in plants, altering the activities of superoxide dismutase, peroxidase, catalase, and ascorbate lyase to limit plant growth (Reyes et al., 2014; Conti et al., 2020), so the growth inhibition of BM is more than that of FAN.

4. Conclusion

In this study, Fe_3O_4/Cu/CuO (FN) was synthesized, and following amination modification, ~3 nm Ag quantum dots (QDs) were loaded onto the surface of FN to synthesize Fe_3O_4/Cu/CuO@Ag (FAN), The application potential of Bordeaux mixture (BM) is examined using its practical application as an indication. Bacteriostatic studies revealed that the nanocomposite FAN material inhibited *E. coli* and *S. aureus* after 20 min at a concentration of 200 μg/mL, which was more than ten times that of BM at the same concentration, and it was more sensitive to *S. aureus*. The results of the inhibition mechanism demonstrate that the material can significantly kill bacteria and severely damage the bacterial cell wall, and that its toxicity to lactating cells is 10 % that of BM. When the concentration is less than 200 μg/mL, it can considerably improve mung bean germination, root activity, and chlorophyll content, and its application performance is twice that of BM. In a nutshell, the best FAN concentration is its potential value as a replacement for Bordeaux in agricultural planting.

5. Contributions

SBG helped in design, synthetic materials, analysis, investigation, writing original draft, writing review and editing. ZD,YMQ, HTX, JFL, ZFL, JS contributed to characterized the materials and analyzed the data, XHJ and TLZ provided help for conceptualization, funding acquisition, supervision, writing review and editing.

CRediT authorship contribution statement

Shaobo Guo: Investigation, Writing – original draft, Writing –

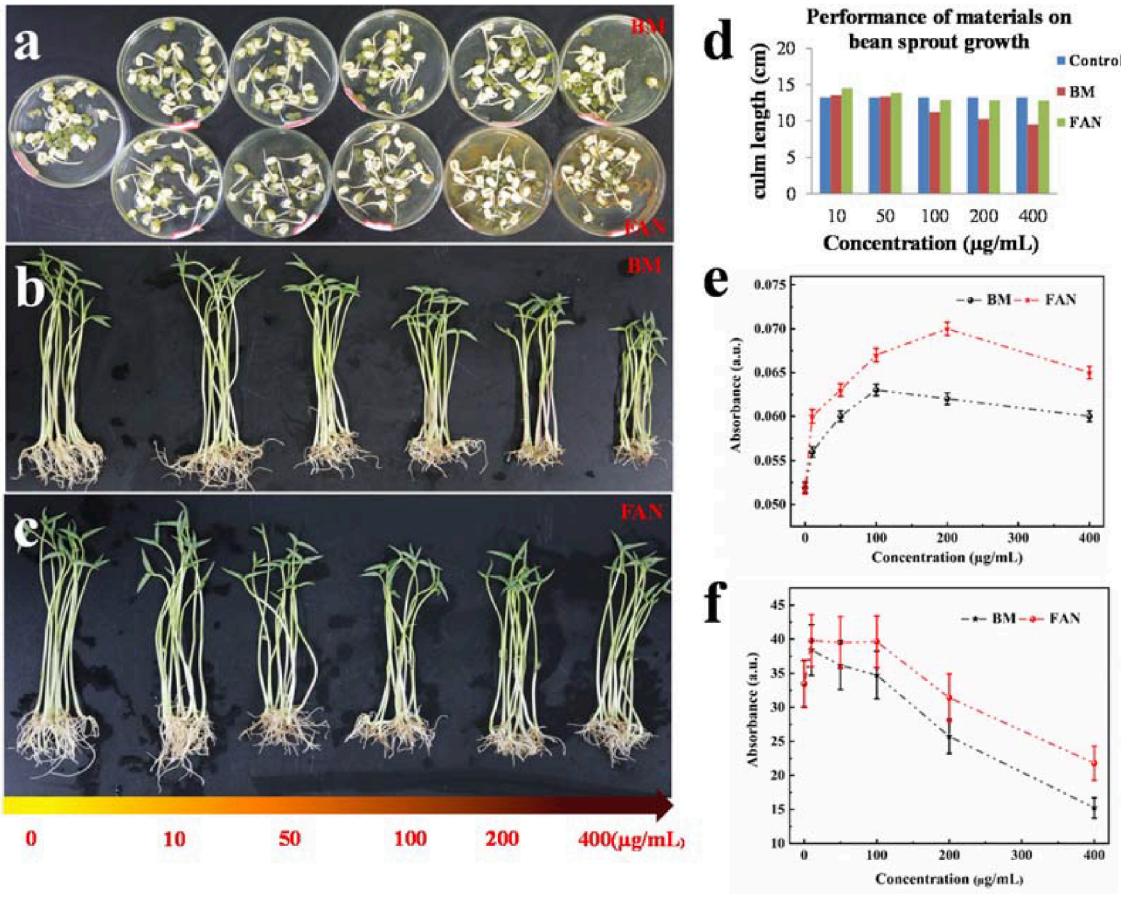

Fig. 6. Photographs of the results of FAN and BM on mung bean sprouting (a). Photographs of the results of the effect of materials on root activity and chlorophyll content during the growth of mung bean (b, c) and corresponding data analysis results (d-f).

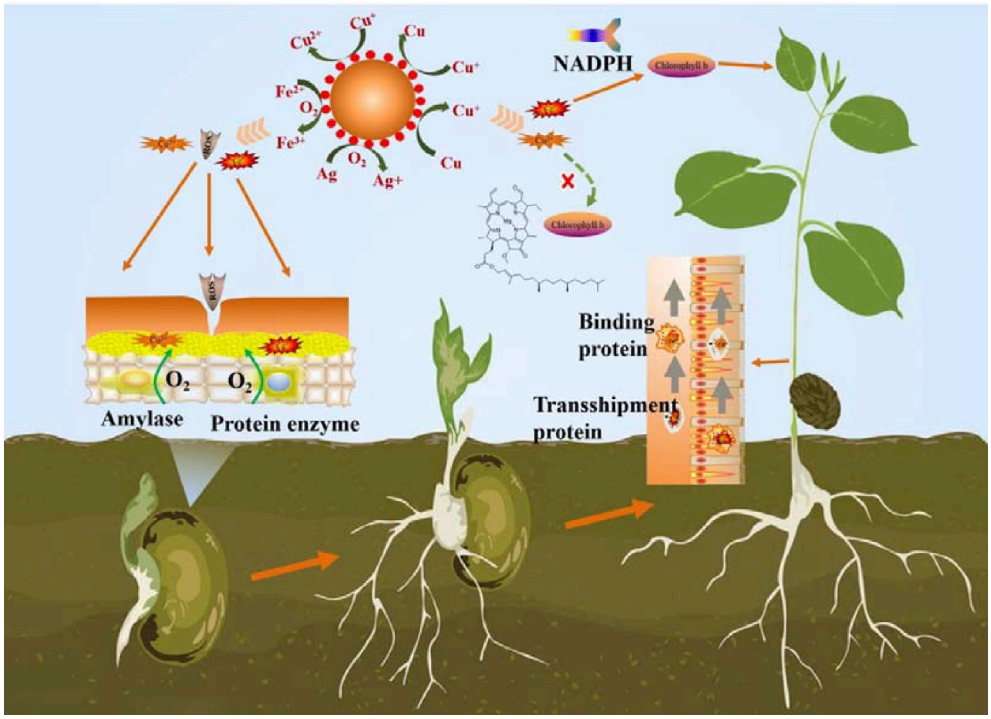

Fig. 7. Plant growth mechanism diagram.

review & editing. **Zhang Dan: . Yanming Qiao: . Haitao Xu: . Jiufu Lu: . Zhifeng Liu: . Juan Shi: . Xiaohui Ji:** Conceptualization, Funding acquisition, Supervision, Writing – review & editing. **Tanlei Zhang:** Conceptualization, Funding acquisition, Supervision, Writing – review & editing.

Declaration of competing interest

The authors declare that they have no known competing financial interests or personal relationships that could have appeared to influence the work reported in this paper.

Acknowledgments

The Scientific Research Foundation of State Key Laboratory of Qinba Bio-Resource and Ecological Environment (SXC-2105), Shaanxi Provincial Natural Science Foundation (2023-JC-QN-0162, 2022JQ-148, 2021JQ-756), the Shaanxi Provincial Department of Education Project (22JK0311), and the Fundamental Research Funds of Shaanxi University of Technology (SLGKYXM2208) provided financial support for this work.

Appendix A. Supplementary material

Supplementary data to this article can be found online at https://doi.org/10.1016/j.arabjc.2023.105524.

References

An, X.D., Erramilli, S.S., Reinhard, B.M., 2021. Plasmonic nano-antimicrobials: properties, mechanisms and applications in microbe inactivation and sensing. Nanoscale 13, 3374–3411.

Banakar, R., Fernández, Á.A., Abadía, J., Capell, T., Christou, P., 2017. The expression of heterologous Fe (III) phytosiderophore transporter HvYS1 in rice increases Fe uptake, translocation and seed loading and excludes heavy metals by selective Fe transport. Plant Biotechnol. J. 15, 423–432.

Belmonte, I.D.S., Pizzolato, T.M., Gama, M.R., 2022. Guaternary ammonium pesticides: A review of chromatography and non-chromatography methods for determination of pesticide residues in water samples. Trends. Environ. Anal. 35, e00171.

Benarroch, J., Asally, M., 2020. The microbiologist's guide to membrane potential dynamics. Trends. Microbiol. 28, 304–314.

Cao, C.Y., Zhang, T.B., Yang, N., Niu, X.H., Zhou, Z.B., Wang, J.N., Yang, D.L., Chen, P., Zhong, L.P., Dong, X.C., Zhao, Y.X., 2022. POD Nanozyme optimized by charge separation engineering for light/pH activated bacteria catalytic/photodynamic therapy. Sig. Transducti. Tar. 7, 1–9.

Conti, L.D., Cesco, S., Mimmo, T., Pii, Y., Valentinuzzi, F., Melo, G.W.B., Ceretta, C.A., Trentin, E., Anderson, C.R.M., Brunetto, U.G., 2020. Iron fertilization to enhance tolerance mechanisms to copper toxicity of ryegrass plants used as cover crop in vineyards. Chemosphere 243, 125298.

Cota, R.K., Ye, Y.Q., Valdes, C., Deng, C.Y., Wang, Y., Hernández, V.J., Duarte, G.M., Gardea, T.J., 2020. Copper nanowires as nanofertilizers for alfalfa plants: Understanding nano-bio systems interactions from microbial genomics, plant molecular responses and spectroscopic studies. Sci. Total. Environ. 742, 140572.

Deng, M.Y., Zhang, M., Huang, R., Li, H.Y., Lv, W.X., Lin, X.J., Huang, R.Q., Wang, Y., 2022. Diabetesimmunity-modulated multifunctional hydrogel with cascade enzyme catalytic activity for bacterial wound treatment. Biomaterials 289, 121790.

Ding, R.G., Li, W.Q., He, C.S., Wang, Y.R., Liu, X.C., Zhou, G.N., Mu, Y., 2021. Oxygen vacancy on hollow sphere $CuFe_2O_4$ as an efficient Fenton-like catalysis for organic pollutant degradation over a wide pH range. Appl. Catal. B-Environ. 291, 120069.

Du, W.C., Tan, W.J., Yin, Y., Ji, R., Peralta, V.J.R., Guo, H.Y., Gardea, T.J.L., 2018. Differential effects of copper nanoparticles/microparticles in agronomic and physiological parameters of oregano (Origanum vulgare). Sci. Total. Environ. 618, 306–312.

Gilroy, K.D., Ruditskiy, A., Peng, H.C., Qin, D., Xia, Y.N., 2016. Bimetallic nanocrystals: syntheses, properties, and applications. Chem. Rev. 116, 10414–10472.

He, J., Hong, M., Xie, W.Q., Chen, Z., Chen, D.M., Xie, S.Y., 2022. Progress and prospects of nanomaterials against resistant bacteria. J. Control. Release. 351, 301–323.

Imani, S.M., Ladouceur, L., Marshall, T., Maclachlan, R., Soleymani, L., Didar, T.F., 2020. Antimicrobial nanomaterials and coatings: current mechanisms and future perspectives to control the spread of viruses including SARS-CoV-2. ACS Nano 14, 12341–12369.

Jang, J.H., Lee, J.M., Oh, S.B., Choi, Y.Y., Jung, H.S., Choi, J.H., 2020. Development of antibiofilm nanocomposites: Ag/Cu bimetallic nanoparticles synthesized on the surface of graphene oxide nanosheets. ACS Appl. Mater. Inter. 12, 35826–35834.

King, D.W., Berger, E., Helm, Z., Irish, E., Mopper, K., 2016. Measurement of antioxidant activity toward superoxide in natural waters. Front. Mar. Sci. 3, 217.

K.C. Li, M.X. Fu, L.C. Ma, H.X Yang, Q.L. Li. Zero-valent iron drives the passivation of Zn and Cu during composting: Fate of heavy metal resistant bacteria and genes, Chem. Eng. J., 452 (2022) 139136.

Li, Q.Q., Wang, F., Shi, L., Tang, Q.R., Li, B.X., Wang, X.B., Jin, Y., 2022. Nanotrains of DNA copper nanoclusters that triggered a cascade fenton-like reaction and glutathione depletion to doubly enhance chemodynamic therapy. ACS Appl. Mater. Inter. 14, 37280–37290.

Liu, Z.L., Gao, W.Z., Liu, L.Z., Luo, S.J., Zhang, C., Yue, T.L., Sun, J., Zhu, M.Q., Wang, J. L., 2022. Work function mediated interface charge kinetics for boosting photocatalytic water sterilization. J. Hazard. Mater. 442, 130036.

Liu, Z.F., Guo, S.B., Fang, X., Shao, X.Z., Zhao, Z.P., 2022. Antibacterial and plant growth-promoting properties of novel Fe_3O_4/Cu/CuO magnetic nanoparticles. RSC Adv. 12, 19856–19867.

Mikel, R.I., Rodrigo, I., Berganza, L.B., Serea, E.S.A., Plazaola, F., Senentxu, L.M., Erlantz, L., Javier, R., 2022. Core–shell Fe_3O_4@Au nanorod-loaded gels for tunable and anisotropic magneto- and photothermia. ACS Appl. Mater. Inter. 14, 7130–7140.

Nieto, M.A., Bustos, G.S., Espinoza, G.H., Flores, L.L.Z., Ramirez, A.K., Alonso, N.G., Cadena, N.R.D., 2022. Green synthesis of copper nanoparticles using different plant extracts and their antibacterial activity. J. Environ. Chem. Eng. 10, 2213–3437.

Nilanjan, C., Jishnu, B., Pallab, C., Anuron, B., Sumeddha, C., Kasturi, R., Krishnendu, A., Joy, S., 2022. Green synthesis of copper/copper oxide nanoparticles and their applications: a review. Green Chem. Lett. Rev. 15, 1751–8253.

Rana, J.D., Guilherme, A.G.R., Nicole, C., Geoffrey, S., Clara, B., Fredy, B., Magda, B.D. K., Christophe, B., 2022. Intracellular reactive oxygen species trafficking participates in seed dormancy alleviation in arabidopsis seeds. New Phytol. 234, 850–866.

Reyes, T., Botez, M., Videa, P., Torresdey, G., 2014. Exposure studies of core–shell Fe/Fe_3O_4 and Cu/CuO NPs to lettuce (Lactuca sativa) plants: Are they a potential physiological and nutritional hazard. J. Hazard. Mater. 267, 255–263.

Sami, R., Stephanos, K., Nikolay, B., Victor, N., Inessa, K., John, K., 2020. New evidence for Ag-sputtered materials inactivating bacteria by surface contact without the release of Ag ions: end of a long controversy? ACS Appl. Mater. Inter. 12, 4998–5007.

Sen, S., Won, M., Levine, M.S., Noh, Y., Sedgwick, A.C., Kim, J.S., Sessler, J.L., Arambula, J.F., 2022. Metal-based anticancer agents as immunogenic cell death inducers: the past, present, and future. Chem. Soc. Rev. 51, 1212–1233.

Wang, F.B., Chen, Z.H., Wang, Y.Y., Ma, C.Y., Bi, L., Song, M.Y., Jiang, G.B., 2022. Silver nanoparticles induce apoptosis in hepG2 cells through particle-specific effects on mitochondria. Environ. Sci. Technol. 56, 5706–5713.

Wang, Y., Zheng, Y.Q., Huang, C.Z., Xia, Y.N., 2013. Synthesis of Ag nanocubes 18–32 nm in edge length: the effects of polyol on reduction kinetics, size control, and reproducibility. J. Am. Chem. Soc. 135, 1941–1951.

Wu, Y.B., Han, S.B., Li, Y., Shen, W.J., 2022. Fabrication of monodisperse gold-copper nanocubes and AuCu-cuprous sulfide heterodimers by a step-wise polyol reduction. J. Colloid. Interf. Sci. 626, 136–145.

Yeon, J., Park, A.R., Nguyen, H.T.T., Gwak, H., Kim, J.W., Sang, M.K., Kim, J.C., 2022. Inhibition of oomycetes by the mixture of maleic acid and copper sulfate. Plant Dis. 106, 960–965.

Yu, N.X., Wang, X.Y., Qiu, L., Cai, T.M., Jiang, C.J., Sun, Y., Li, Y.B., Peng, H.L., Xiong, H., 2020. Bacteria-triggered hyaluronan/AgNPs/gentamicin nanocarrier for synergistic bacteria disinfection and wound healing application. Chem. Eng. J. 380, 122582.

Yu, S.M., Wang, Y.N., Shen, F., Fang, H., Yu, Y.L., 2022. Copper-based fungicide copper hydroxide accelerates the evolution of antibiotic resistance via gene mutations in *Escherichia coli*. Sci. Total. Environ. 815, 152885.